Ruijie Liu,[1] Yifei Zhong,[2] Xuezhu Li,[3] Haibing Chen,[4] Belinda Jim,[5] Ming-Ming Zhou,[6] Peter Y. Chuang,[1] and John Cijiang He[1,7]

Role of Transcription Factor Acetylation in Diabetic Kidney Disease

Diabetes 2014;63:2440–2453 | DOI: 10.2337/db13-1810

Nuclear factor (NF)-κB and signal transducer and activator of transcription 3 (STAT3) play a critical role in diabetic nephropathy (DN). Sirtuin-1 (SIRT1) regulates transcriptional activation of target genes through protein deacetylation. Here, we determined the roles of Sirt1 and the effect of NF-κB (p65) and STAT3 acetylation in DN. We found that acetylation of p65 and STAT3 was increased in both mouse and human diabetic kidneys. In human podocytes, advanced glycation end products (AGEs) induced p65 and STAT3 acetylation and overexpression of acetylation-incompetent mutants of p65 and STAT3 abrogated AGE-induced expression of NF-κB and STAT3 target genes. Inhibition of AGE formation in db/db mice by pyridoxamine treatment attenuated proteinuria and podocyte injury, restored SIRT1 expression, and reduced p65 and STAT3 acetylation. Diabetic db/db mice with conditional deletion of *SIRT1* in podocytes developed more proteinuria, kidney injury, and acetylation of p65 and STAT3 compared with db/db mice without *SIRT1* deletion. Treatment of db/db mice with a bromodomain and extraterminal (BET)-specific bromodomain inhibitor (MS417) which blocks acetylation-mediated association of p65 and STAT3 with BET proteins, attenuated proteinuria, and kidney injury. Our findings strongly support a critical role for p65 and STAT3 acetylation in DN. Targeting protein acetylation could be a potential new therapy for DN.

Diabetic nephropathy (DN) is the most common cause of end-stage renal disease (ESRD) in the U.S., and its incidence has been increasing worldwide over the past decade (1). Current interventions provide only partial therapeutic effects, and therefore it is critical to develop more effective therapy for DN.

Many studies have suggested a role for advanced glycation end products (AGEs) in the pathogenesis of DN. Nondiabetic animals infused with AGEs develop histological changes similar to those found in animals with DN (2,3). Reduction of AGE accumulation by lowering dietary AGE consumption or by pharmacologic inhibition of AGE formation has been shown to ameliorate microvascular diseases and DN in animal models (2,4,5). We have demonstrated previously that both circulating and matrix-bound AGEs cause podocyte apoptosis through activation of the receptor for AGE (6).

Multiple transcription factors (TFs) that are activated under the diabetic condition also are known to mediate hyperglycemia- and AGE-induced pathologic changes in DN. Systems-based analyses of gene expression patterns in the diabetic kidney suggest that Janus kinase–signal transducer and activator of transcription (JAK/STAT) and nuclear factor (NF)-κB signaling are major pathways activated in the kidneys of humans with DN (7,8). We demonstrated previously that FOXO4 is a major TF that mediates AGE-induced podocyte apoptosis by activating

[1]Department of Medicine/Nephrology, Mount Sinai School of Medicine, New York, NY
[2]Department of Nephrology, Longhua Hospital, Shanghai University of Traditional Chinese Medicine, Shanghai, China
[3]Department of Nephrology, Shanghai East Hospital, Tongji University School of Medicine, Shanghai, China
[4]Department of Endocrinology, Shanghai Jiao Tong University Affiliated Sixth People's Hospital, Shanghai, China
[5]Division of Nephrology, Jacobi Medical Center, Bronx, NY
[6]Department of Structural and Chemical Biology, Mount Sinai School of Medicine, New York, NY
[7]Renal Section, James J. Peters VA Medical Center, Bronx, NY

Corresponding author: John Cijiang He, cijiang.he@mssm.edu.

Received 27 November 2013 and accepted 10 February 2014.

This article contains Supplementary Data online at http://diabetes.diabetesjournals.org/lookup/suppl/doi:10.2337/db13-1810/-/DC1.

R.L. and Y.Z. contributed equally to this work.

See accompanying article, p. 2432.

Bim-1, a proapoptotic protein (6,9). TF activation is typically determined by its phosphorylation status. However, recent evidence suggests that protein acetylation also is required for TF activation. Sirtuin-1 (SIRT1), an enzyme that mediates NAD^+-dependent deacetylation of target substrates, regulates the activity of many TFs by targeting them for deacetylation. SIRT1 regulates the acetylation status of the FOXO family of TFs, thereby affecting their downstream gene expression (10,11). We showed that SIRT1 inhibits podocyte apoptosis by deacetylating FOXO4 (6,9). Several studies suggest that the transcriptional activity of STAT3 also is negatively regulated by SIRT1 (12–15). SIRT1 mediates anti-inflammatory effects by inhibiting NF-κB transcriptional activity via its acetylation-mediated association with bromodomain and extraterminal (BET) bromodomain proteins such as BRD4 (16–18). We found that SIRT1 expression is suppressed by AGE in cultured podocytes and in human diabetic kidneys (9).

Based on these findings, here we attempt to address *1*) the acetylation status of TFs in the diabetic kidney; *2*) the effect of AGE inhibition in diabetic db/db mice on SIRT1 expression, TF acetylation, and podocyte apoptosis; *3*) the role of podocyte SIRT1 in the progression of DN and regulation of TF acetylation; and *4*) the therapeutic effects of bromodomain inhibitors in DN.

RESEARCH DESIGN AND METHODS

Animal Studies

Female db/db and db/m mice (6 weeks old) in C57BLKS background were obtained from The Jackson Laboratory (Bar Harbor, ME). When mice developed hyperglycemia (8 weeks of age), they were randomized to receive either pyridoxamine (PYR; n = 6; 250 mg/kg/day in drinking water; Biostratum Inc., Durham, NC) or vehicle (n = 6). Mice were housed individually, and the concentration of PYR in drinking water was adjusted daily based on the animal's water intake. Floxed *SIRT1* mice ($SIRT1^{fl/fl}$) were obtained from The Jackson Laboratory. These mice were crossed with podocin (Pod)-$Cre^{+/-}$ mice to generate podocyte-specific *SIRT1* knockout mice (Pod-Cre;$SIRT1^{fl/fl}$). Pod-$Cre^{+/-}$;$SIRT1^{fl/fl}$ mice were further crossed with db/db mice to generate Pod-$Cre^{+/-}$;$SIRT1^{fl/fl}$;db/m mice, which were further crossed with each other to generate Pod-$Cre^{+/-}$;$SIRT1^{fl/fl}$;db/db mice. Pod-$Cre^{+/-}$;db/db and Pod-$Cre^{+/-}$;db/m mice also were generated. Therefore, 4 groups of mice were included in the study: Pod-$Cre^{+/-}$;$SIRT1^{fl/fl}$;db/db, Pod-$Cre^{+/-}$;$SIRT1^{fl/fl}$;db/m, Pod-$Cre^{+/-}$;db/db, and Pod-$Cre^{+/-}$;db/m.

Diabetic db/db and nondiabetic db/m mice were fed either a control vehicle (DMSO) or MS417 by daily gavage at a concentration of 0.08 mg/kg, as described previously (19). The mice (n = 6) were fed with this compound daily from the age of 8 weeks to 20 weeks. Unrestricted food and water were provided throughout the duration of the experiment. The mice were killed at 20 weeks of age.

For all experiments, glycemia and glycosuria were monitored in diabetic animals twice per week. After the mice were killed, blood, urine, and kidney tissue were collected. Iron beads were perfused in one kidney for glomerular isolation; the other kidney was perfused with 4% paraformaldehyde for histology and immunostaining. All animal studies were performed according to the protocols approved by the Institutional Animal Care and Use Committee at the Mount Sinai School of Medicine.

Quantification of Urine Albumin

Urine protein was quantified by ELISA for albumin with a kit from Bethyl Laboratories Inc. (Houston, TX). Urine creatinine levels were measured in the same samples. The urine albumin excretion rate is expressed as the ratio of albumin to creatinine.

Histology and Morphological Analysis

Kidney histology was examined after periodic acid Schiff staining. The glomerular volume and mesangial area were determined by examining periodic acid Schiff–stained sections using a digitizing tablet and video camera, as previously described (5). The relative mesangial area was expressed as the mesangial-to-glomerular surface area (percentage).

Isolation of Glomeruli

Glomeruli were isolated by perfusion of ferric oxide, as previously described (20). The purity of the glomeruli isolate was verified under light microscopy and by Western blot for podocyte-specific markers, as described elsewhere (6,21).

Immunostaining

Paraffin-embedded sections of mouse and human kidneys were incubated with primary antibodies and then with biotinylated second antibodies, followed by incubation with an avidin–biotin–peroxidase complex; they were developed using substrate provided by Vector Laboratories. The human biopsy and nephrectomy samples were obtained under a protocol approved by the institutional review board of Icahn School of Medicine at Mount Sinai (HS#: 11–02130). The following antibodies were used in the study: SIRT1 (cat. no. 07131; Millipore), acetyl-STAT3 (cat. no. 2523; Cell Signaling Technology), phosphor-STAT3 (cat. no. 9145; Cell Signaling Technology), acetyl-p65 (cat. no. 3045; Cell Signaling Technology), phosphor-p65 (cat. no. 3033; Cell Signaling Technology), and synaptopodin (provided courtesy of Dr. Peter Mundel). The dilutions of both acetyl-p65 and acetyl-STAT3 antibodies for immunostaining were 1:50. Negative controls for acetyl-STAT3 and acetyl-p65 were obtained by preabsorption with a synthetic acetylated peptide corresponding to residues surrounding Lys310 of p65 or Lys685 of STAT3.

Quantification of Immunostaining

ImageJ 1.26t software was used to measure the level of immunostaining in the glomeruli. First, the images were converted to 8-bit grayscale. Next, the glomerular region was selected for measurement of area and integrated density. Then, the background intensity was measured by selecting three distinct areas in the background with no staining. The corrected optical density was determined as

shown in the equation: corrected optical density = ID − (A × MGV), where *ID* is the integrated density of the selected glomerular region, *A* is the area of the selected glomerular region, and *MGV* is the mean gray value of the background readings (21). Synaptopodin staining was quantified by counting the percentage of positive staining area per glomerulus. The Sirt1 staining was quantified by counting the number of positively stained cells per glomerulus.

Podocyte Culture

Conditionally immortalized human podocytes (courtesy of Dr. Moin Saleem, Bristol, U.K.) were cultured as described previously (22). Endotoxin-free AGE-BSA was prepared from endotoxin-free, lyophilized BSA (fraction IV; Sigma) and glucose, as described previously (6). AGE levels were measured by ELISA, as described previously by Makita et al. (23).

Mutagenesis

Human *STAT3* cDNA plasmid was purchased from Open Biosystems (clone ID 3347434). The K685R mutation was generated following the Stratagene Site-Directed Mutagenesis protocol. The mutant primer sequence is 5′-CTC TGG CCG ACA ATA CCT TCC GAA TGC CTC CTC-3′. The wild-type and mutant full-length *STAT3* sequences were amplified using a forward primer with a *Bam*^{1}H cutting site (5′-TTG GAT CCG CCA CCA TGG CCC AAT GGA ATC AGC TAC-3′) and a reverse primer with an Xma1 cutting site (5′-CCG GCC CGG GTC ACA TGG GGG AGG TAG CGC-3′). PCR product then was cloned, first into a T-vector (Promega A1360) and finally into a pHR-CMV-MCS-IRES-gfp-delta B vector using *Bam*^{1}H and Xma1. Human wild-type and K310R mutant *p65* plasmids were also generated. PCR product was obtained with the following primers: 5′-CTA GAC TAG TTT AGG TGC TGA TCT GAC TCA-3′ (sense) and 5′-TAG ATA TCT TAG GAG CTG ATC TGA CTC AGC-3′ (antisense). The strategy of cloning into pHR-CMV-MCS-IRES-gfp-delta B vector was the same as that of *STAT3*, except endonucleases were used for *Bam*^{1}H (5′ end) and Sma1 (3′ end).

Viral Preparation

Using the PolyJet transfection method, 50% confluent 293T cells were transfected with the following three plasmids: 1 μg pVSV.G, 2 μg pPACK together with 3 μg gene of interest plasmid of either empty pHR-CMV-MCS-IRES-gfp-delta B vector, or wild-type STAT3, or K685R STAT3, or wild-type p65, or K310R p65 plasmid. Medium containing viral particles was centrifuged at 5,000 rpm for 4 h at 4°C. The pellet was dissolved in 1 mL serum-free RPMI medium.

Apoptosis Assay

TUNEL fluorescent staining (Millipore) was used to determine the apoptosis rate in kidney sections of mice. We counted all glomeruli with at least one apoptotic podocyte, and the percentage of glomeruli with apoptotic cells was shown as described previously (24). At least 100 glomeruli per mouse were examined.

Real-Time PCR

Quantitative reverse-transcriptase PCR was performed using Sybr Green Master Mix (Applied Biosystems). The $2^{-\Delta\Delta C_P}$ method was used for the analysis of relative gene expression. Primers were designed using Primer-Blast (National Center for Biotechnology Information, Bethesda, MD) to span at least one intron; the sequences of these primers are listed in Supplementary Table 1. Gene expression was normalized to *GAPDH* as a housekeeping gene.

Western Blot

Nuclear proteins were extracted from glomeruli in a buffer containing a protease inhibitor cocktail and tyrosine and serine-threonine phosphorylation inhibitors. Immunoblotting was performed using the same specific antibodies as described above for immunostaining. The antibody for β-actin was from Sigma (cat. no. a2228). Densitometry analysis for quantification of Western blots was performed as described previously (25).

Chromatin Immunoprecipitation Assay

Human podocytes were infected with the following viruses: green fluorescent protein, wild-type and K658R STAT3 or green fluorescent protein, wild-type and K310R p65 (1:100 V/V) for 3 days and then treated with either AGE-BSA (100 μg/mL) or BSA (100 μg/mL) for an additional 24 h. Chromatin immunoprecipitation assay was performed according to the EZ-CHIP protocol (Millipore catalog no. 17–371) (26). Immunoprecipitated DNA samples were subjected to PCR analysis, normalized to input, and expressed as a percentage of input.

Reporter Gene Assay

Podocytes were transfected with luciferase reporter vectors for NF-κB or STAT3, as described by Zhang et al. (19). Luciferase activity was measured using a luminometer, and the data were normalized for the amount of protein.

Statistical Analysis

Data are expressed as mean ± standard deviation. The unpaired *t* test was used to analyze data between two groups. ANOVA followed by Bonferroni correction was used when more than two groups were present. All experiments were repeated at least three times, and representative experiments are shown. *P* values <0.05 were considered statistically significant.

RESULTS

Acetylation of TFs Is Increased in Diabetic Kidneys

We previously found that acetylation of FOXO4 was significantly increased in the kidney of diabetic db/db mice compared with nondiabetic db/m mice (9). Here, we demonstrated that staining of both acetyl-p65 and acetyl-STAT3 was significantly higher in glomeruli of diabetic db/db mice compared with those of nondiabetic db/m mice (Fig. 1*A* and *B*). Western blots of isolated glomeruli from these mice revealed a higher level of phosphorylation and acetylation for p65 and STAT3 in diabetic db/db mice compared with db/m mice (Fig. 1*C* and *D* and Supplementary

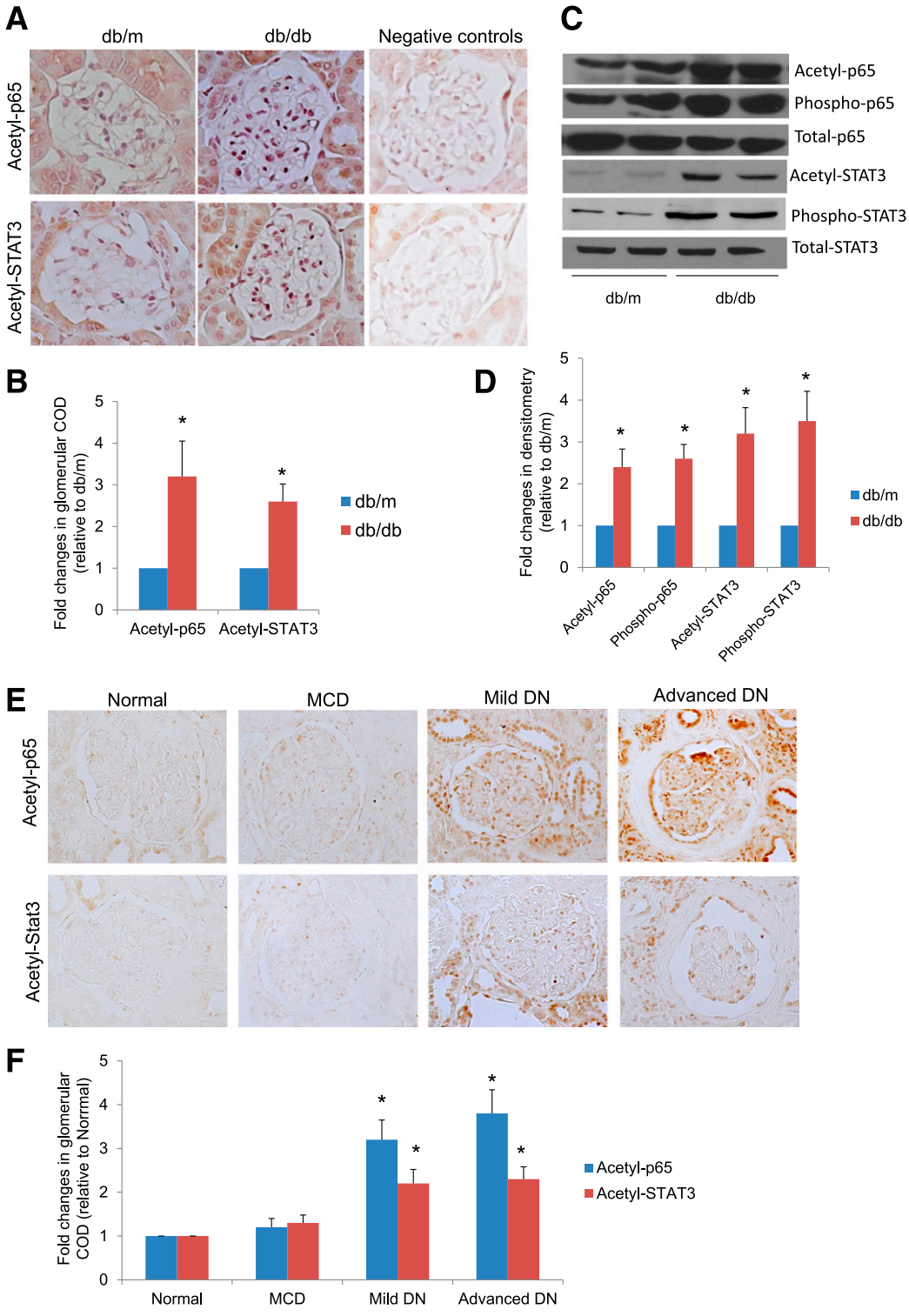

Figure 1—Acetylation of p65 and STAT3 is increased in diabetic kidneys. *A*: Kidney sections from db/db and db/m mice were stained for acetyl-p65 and acetyl-STAT3 using specific antibodies. The representative pictures of six mice in each group are shown. *B*: Immunostaining was quantified as described in RESEARCH DESIGN AND METHODS. *$P < 0.01$ compared with db/m mice ($n = 6$). COD, corrected optical density. *C*: Western blot analyses of glomerular lysates from db/db and db/m mice were performed for acetyl-, phosphor-, and total p65 and STAT3. The representative blots of three independent experiments are shown. *D*: Western blots from all experiments were quantified by densitometry analysis, as described in RESEARCH DESIGN AND METHODS. The ratios of acetyl-protein or phosphor-protein to total protein were calculated for p65 and STAT3. The fold changes relative to db/m mice are shown. *$P < 0.01$ compared with db/m mice ($n = 6$). *E*: Kidney sections from nephrectomized samples of patients with normal kidneys, minimal change disease (MCD), and mild and advanced DN were stained for acetyl-STAT3 and NF-κB. The representative pictures are shown ($n = 5$). *F*: The quantitation data of immunostaining in kidney biopsies from patients with normal kidneys, MCD, mild DN, and advanced DN are shown. *$P < 0.05$ compared with normal and MCD ($n = 5$).

Fig. 1). Immunostaining of kidney biopsy samples revealed that acetylation of p65 and STAT3 was increased in both glomerular and tubular compartments of kidneys of patients with DN compared with patients with minimal change disease and normal kidney tissues from nephrectomy patients (Fig. 1*E* and *F*). The clinical characteristics of these patients are summarized in Supplementary Table 2.

NF-κB and STAT3 Acetylation Is Required for Transcriptional Activation of Target Genes

Since we have previously shown that AGE suppresses SIRT1 expression in podocytes (9), here we tested whether AGE increases the acetylation of these TFs in podocytes. Using Western blot analysis, we found that AGE treatment induced both phosphorylation and acetylation of p65 and STAT3 in podocytes compared with BSA treatment (Fig. 2*A* and *B*). These data, together with our previous findings, suggest that AGE likely induces the acetylation of p65 and STAT3 by inhibiting SIRT1 expression.

To confirm that acetylation of p65 and STAT3 is required for the transcriptional activation of their target genes, we generated mutants of *p65* (K310R) and *STAT3* (K685R), in which the major acetylated lysine residues were mutated. First, we confirmed the overexpression of these mutants in podocytes by Western blot analysis (Fig. 2*C–F*). We confirmed that overexpression of these mutants in podocytes inhibited tumor necrosis factor-α–induced NF-κB activation and interleukin-6–induced STAT3 activation as measured by luciferase reporter assays (Fig. 2*G* and *H*). Then, we found that overexpression of these mutants in podocytes suppressed AGE-induced expression of NF-κB and STAT3 target genes as measured by real-time PCR (Fig. 3*A–D*), thus confirming that acetylation of NF-κB and STAT3 is required for their transcriptional activation in podocytes. We selected *CXCL5* and *CCL17* as NF-κB target genes and *SOC3* and *Casp9* as STAT3 target genes based on previous studies (9).

Next, we determined whether acetylation of p65 and STAT3 is required for protein-DNA binding of TFs to the promoter of their target genes. Using chromatin immunoprecipitation assay, we found that AGE-induced binding of p65 and STAT3 in the promoter sites of their target genes were markedly inhibited by the overexpression of *p65* (K310R) and *STAT3* (K685R) in podocytes (Fig. 3*E–H*). These data further support the critical role of acetylation in the transcriptional regulation of NF-κB and STAT3 target genes in AGE-treated podocytes.

PYR Restores Sirt1 Expression and Reduces TF Acetylation in Diabetic db/db Mice

Next we determined whether the inhibition of AGE formation in db/db diabetic mice using a specific AGE inhibitor, PYR, restores Sirt1 expression, reduces TF acetylation, and attenuates podocyte apoptosis and proteinuria in diabetic db/db mice. In Supplementary Table 3, we summarize the body weight, kidney weight, and blood glucose concentrations of db/m and db/db mice treated with either vehicle or PYR. We found that the kidney weights of db/db mice treated with vehicle were higher than db/m mice treated with vehicle, but kidney hypertrophy was prevented in db/db mice treated with PYR. Diabetic db/db mice treated with vehicle developed significant proteinuria, glomerular hypertrophy, mesangial expansion, and podocyte loss compared with nondiabetic db/m mice (Fig. 4*A–G*). However, db/db mice treated with PYR developed less proteinuria, glomerular hypertrophy, mesangial expansion, and podocyte loss than db/db mice treated with vehicle (Fig. 4*A–G*). SIRT1 expression was partially restored in the glomeruli of db/db mice treated with PYR but not in db/db mice treated with vehicle (Fig. 5*A–D*). Consistent with previously findings, synaptopodin expression also was reduced in diabetic kidneys but was restored by PYR treatment (Fig. 5*A–D*). By immunostaining, we found that the acetylation status of both p65 and STAT3 in the glomeruli of db/db mice treated with PYR was lower than that in db/db mice treated with vehicle (Fig. 5*E–H*). Taken together, these data suggest that renal protection afforded by PYR is associated with the restoration of SIRT1 expression and inhibition of TF acetylation. However, whether suppression of SIRT1 and increased TF acetylation contribute to DN remains to be determined.

Mice With Podocyte-Specific Sirt1 Knockout Are More Susceptible to DN

To determine the role of SIRT1 in podocyte injury and the development of DN, we generated podocyte-specific *SIRT1* knockout mice (Pod-Cre$^{+/-}$;SIRT1$^{fl/fl}$) by crossing Pod-Cre$^{+/-}$ mice with mice that are homozygous for a floxed *SIRT1* allele (SIRT1$^{fl/fl}$). Pod-Cre$^{+/-}$;SIRT1$^{fl/fl}$ mice then were bred with db/db mice to generate Pod-Cre$^{+/-}$;SIRT1$^{fl/fl}$;db/m and Pod-Cre$^{+/-}$;SIRT1$^{fl/fl}$;db/db mice, which were used in subsequent experiments. Pod-Cre$^{+/-}$;db/db and Pod-Cre$^{+/-}$;db/m mice were used in the study as the control mice. The body weight, kidney weight, and blood glucose concentrations at the time the mice were killed are summarized in Supplementary Table 4. The kidney weight of Pod-Cre$^{+/-}$;db/db mice was higher than that of Pod-Cre$^{+/-}$;db/m mice, and a further increase was observed in Pod-Cre$^{+/-}$;SIRT1$^{fl/fl}$;db/db mice compared with Pod-Cre$^{+/-}$;db/db mice. By immunostaining, we confirmed that SIRT1 expression was low in Pod-Cre$^{+/-}$;db/db mice and even lower in Pod-Cre$^{+/-}$;SIRT1$^{fl/fl}$;db/m and Pod-Cre$^{+/-}$;SIRT1$^{fl/fl}$;db/db mice when they were compared with Pod-Cre$^{+/-}$;db/m mice (Supplementary Fig. 2*A–C*). Immunostaining of synaptopodin in Pod-Cre$^{+/-}$;db/db and Pod-Cre$^{+/-}$;SIRT1$^{fl/fl}$;db/db mice was markedly less than that in the corresponding nondiabetic controls (Supplementary Fig. 2*A–C*). We found that Pod-Cre$^{+/-}$;db/db mice developed more proteinuria, mesangial expansion, and podocyte loss (Fig. 6*A–D*) than nondiabetic control mice. However, Pod-Cre$^{+/-}$;SIRT1$^{fl/fl}$;db/db mice developed more severe proteinuria, mesangial expansion, and podocyte loss than Pod-Cre$^{+/-}$;db/db mice (Fig. 6*A–D*). These findings suggest that podocyte-specific

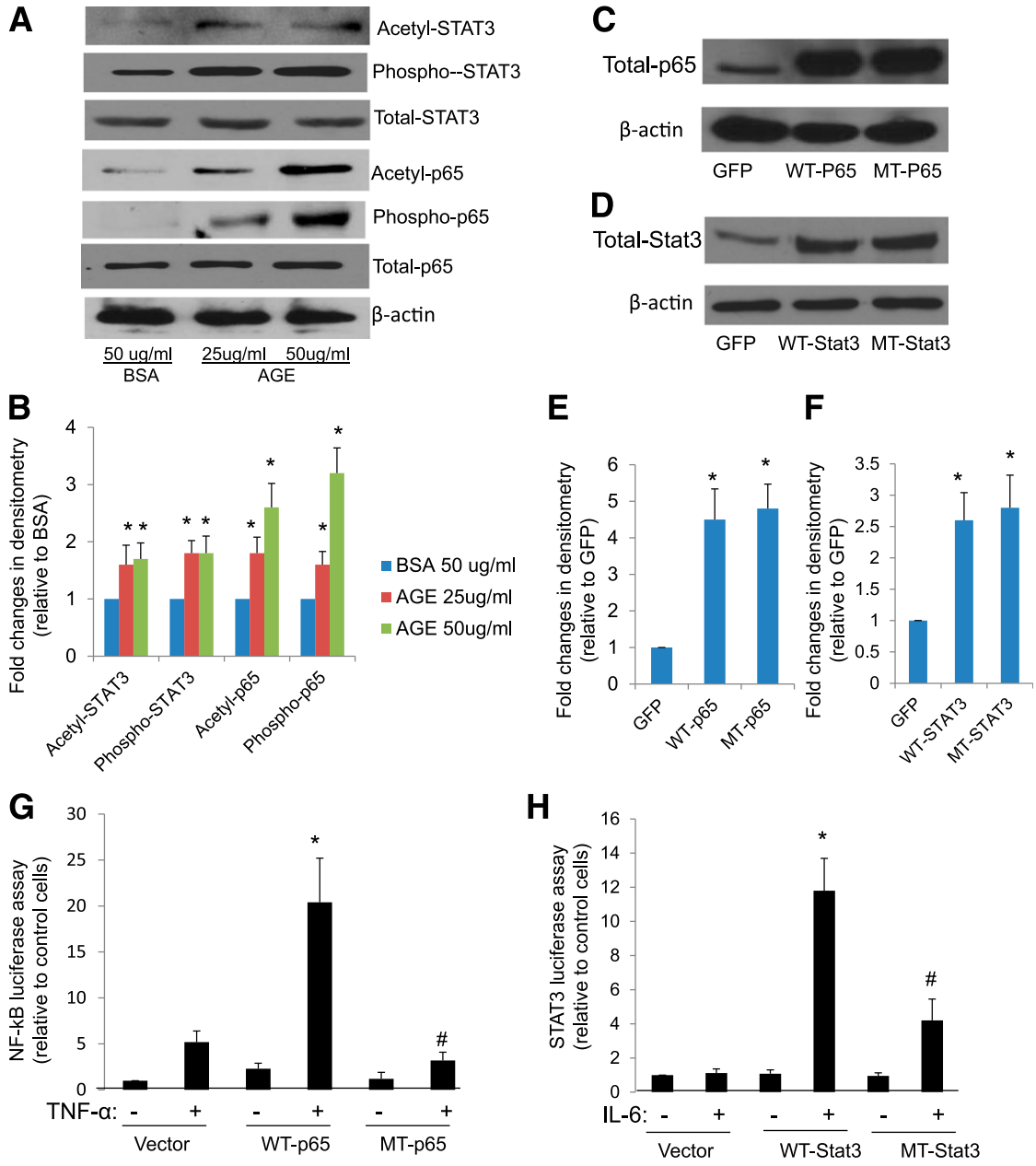

Figure 2—AGE induced acetylation of p65 and STAT3, which is required for their transcriptional activation. *A*: Human podocytes were cultured with AGE or BSA at the indicated doses for 24 h. Cell lysates were subject to Western blot analysis for acetyl-, phosphor-, and total p65 and STAT3. The representative blots of three independent experiments are shown. *B*: The Western blots from all experiments were quantified by densitometry analysis. The ratios of acetyl-protein or phosphor-protein to total protein were calculated for p65 and STAT3. The fold changes relative to BSA-treated cells are shown. **P* < 0.01 compared with BSA-treated cells (*n* = 3). *C* and *D*: Podocytes were infected with wild-type (WT) p65 or STAT3 constructs or p65 and STAT3 constructs with mutated acetyl residues (MT) for 3 days. Western blots were performed to confirm the expression of p65 and STAT3. *E* and *F*: The Western blots from these experiments were quantified by densitometry analysis. The ratios of p65/β-actin (*E*) and STAT3/β-actin (*F*) were calculated; the fold changes relative to cells infected with green fluorescent protein are shown. **P* < 0.01 compared with GFP-infected cells (*n* = 3). *G* and *H*: Podocytes were infected with WT or MT p65 and STAT3 and then transfected with p65 and Stat3 reporter constructs for 3 days. The cells were then further stimulated with either tumor necrosis factor (TNF)-α (10 ng/mL) or interleukin (IL)-6 (10 ng/mL) for an additional 24 h before lysis of cells for measurement of luciferase activity. **P* < 0.01 compared with WT-p65 or WT-STAT3 without TNF-α or IL-6 stimulation; #*P* < 0.05 compared with WT-p65 or WT-STAT3 with TNF-α or IL-6 stimulation (*n* = 3).

knockout of *SIRT1* aggravates podocyte injury and proteinuria in db/db mice. Next we determined the acetylation status of p65 and STAT3 in glomeruli of these mice. By immunostaining, we found that acetylation of p65 and STAT3 was significantly increased in most glomerular cells of Pod-Cre$^{+/-}$;db/db mice compared with nondiabetic control mice (Supplementary Fig. 3*A–D*). However, staining for p65 and STAT3 acetylation seemed to be more pronounced

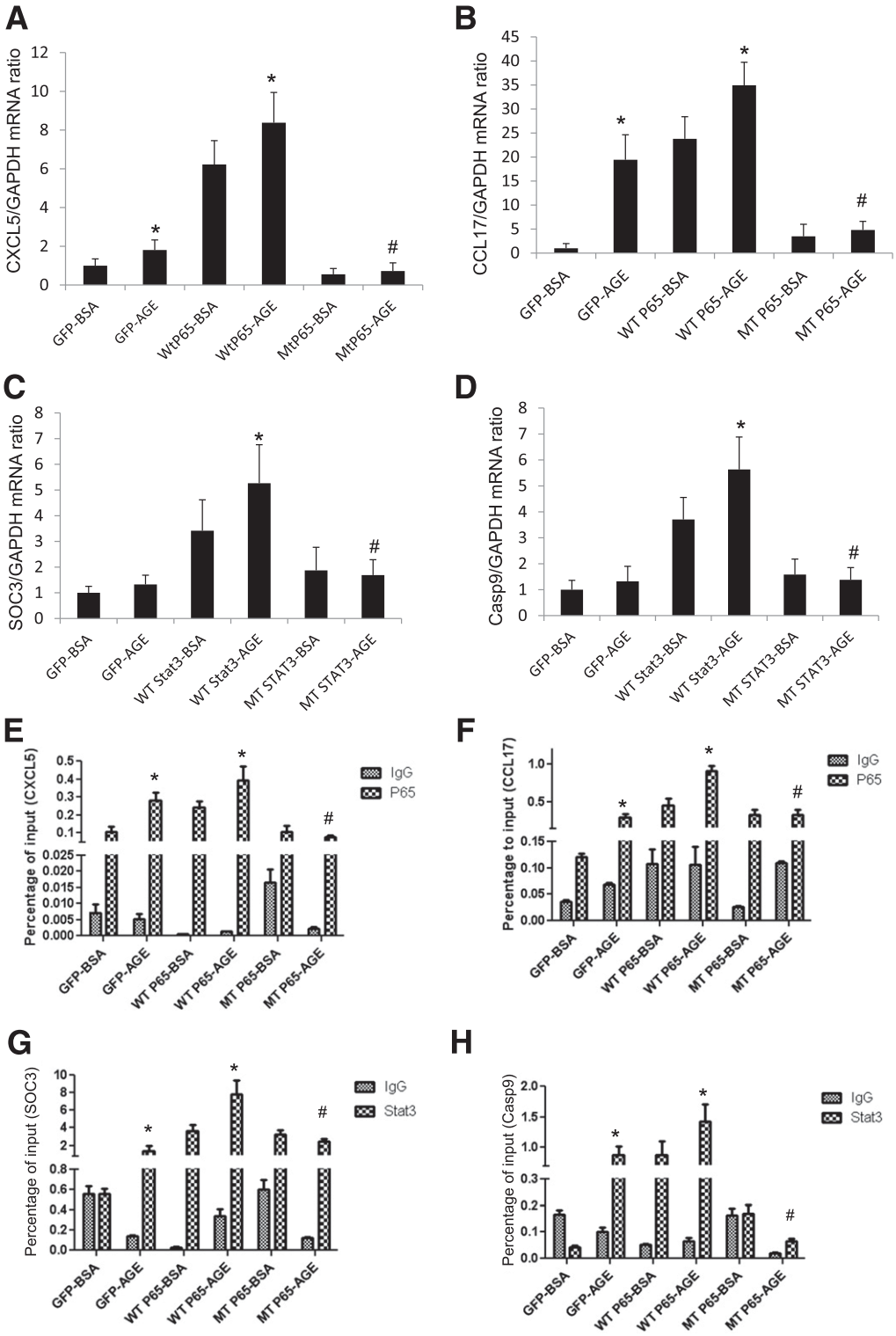

Figure 3—Acetylation of p65 and STAT3 is required for AGE-induced transcriptional activation of their target genes. Podocytes were infected with p65 or STAT3 constructs with mutated acetyl residues for 3 days then stimulated with AGE or BSA at the indicated doses for an additional 24 h. Total RNA was isolated from these cells for real-time PCR analysis of NF-κB target genes (*CXCL5* [*A*] and *CCL17* [*B*]) and STAT3 target genes (*SOC3* [*C*] and *Casp9* [*D*]). For chromatin immunoprecipitation (ChiP) assay for NF-κB and STAT3 target genes, podocytes were infected with p65 or STAT3 constructs with mutated acetyl residues for 3 days then stimulated with AGE or BSA at the indicated doses for an additional 24 h. ChiP assay also was performed in these cells to determine the binding of p65 and STAT3 on the promoter sites of their target genes (*CXCL5* [*E*], *CCL17* [*F*], *SOC3* [*G*], and *Casp9* [*H*]). Immunoprecipitated DNA samples were subjected to PCR analysis and are expressed as a percentage of input. *$P < 0.01$ compared with corresponding BSA-treated cells; #$P < 0.01$ compared with AGE-treated WT-p65 or WT-STAT3 cells ($n = 4$).

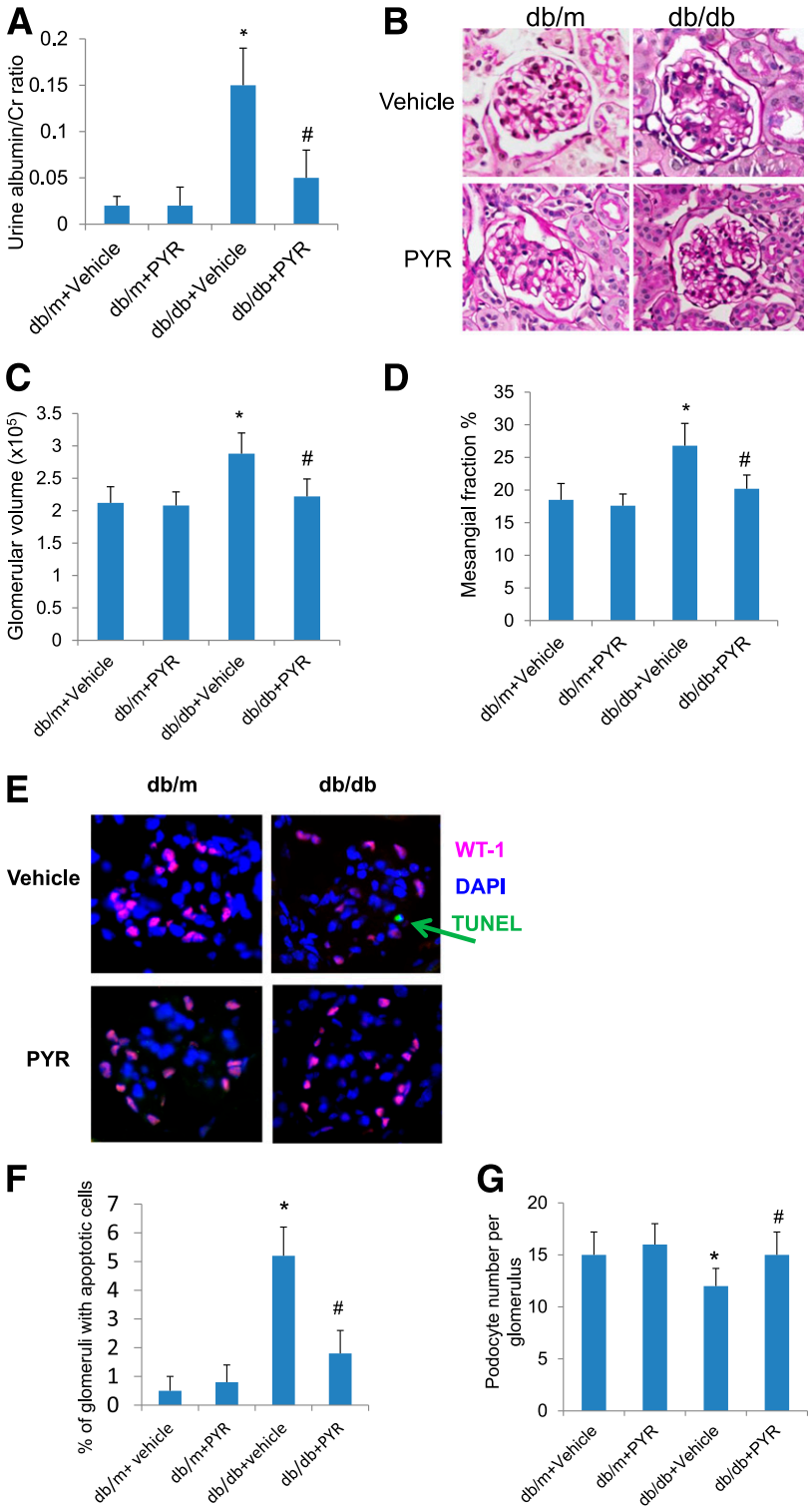

Figure 4—Prevention of AGE formation by PYR attenuates proteinuria and diabetic kidney injury in db/db mice. Eight-week-old female B6 diabetic db/db or nondiabetic db/m mice were randomized to receive either PYR or vehicle for 12 weeks. *A*: Urinary albumin-to-creatinine ratio was measured as described in RESEARCH DESIGN AND METHODS ($P < 0.01$; $n = 6$). *B*: The representative pictures of the kidney histology of these mice are shown after periodic acid Schiff (PAS) staining. Morphometric analysis was performed in these kidney sections with PAS staining for the calculation of glomerular volume (*C*) and mesangial/glomerular fraction area (*D*). Kidney sections also were used for transferase dUTP nick end labeling to determine the rate of apoptosis in podocytes (*E* and *F*) and costained for wild-type 1 (WT-1) to determine the number of podocytes per glomerulus (*E* and *G*). The representative pictures are shown in *E*. *$P < 0.01$ compared with db/m mice treated with vehicle; #$P < 0.05$ compared with db/db mice treated with vehicle ($n = 6$).

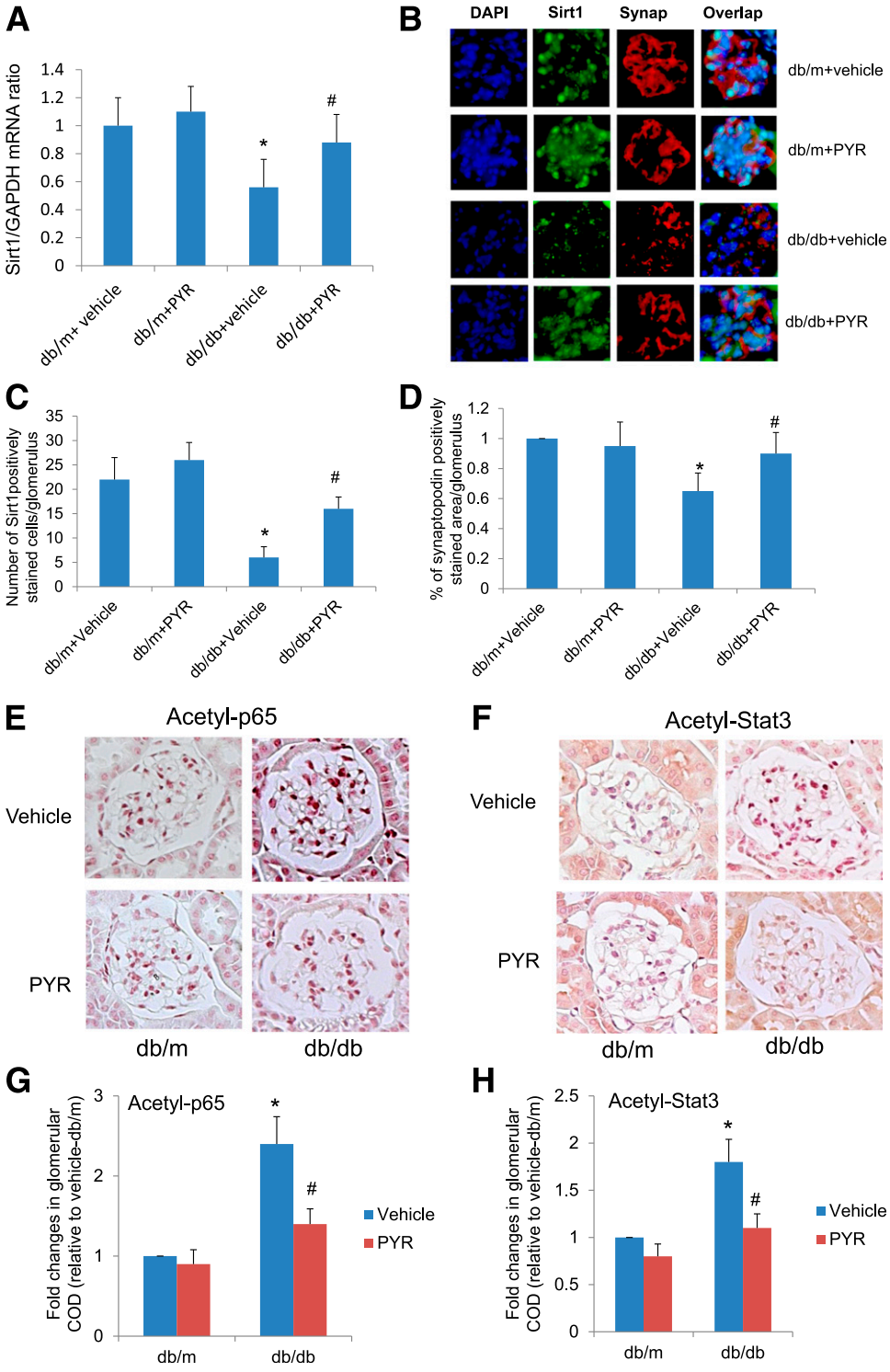

Figure 5—Treatment of db/db mice with PYR restores SIRT1 expression and reduces acetylation of p65 and STAT3 in the kidney of db/db mice. *A*: mRNA levels of SIRT1 were assessed by real-time PCR. *B*: Immunofluorescence staining for SIRT1 and synaptopodin was performed in kidney sections of these mice. *C*: SIRT1 staining was quantified by counting the number of cells stained positively for SIRT1 and colocalized with synaptopodin per glomerulus. *D*: Synaptopodin staining was quantified by calculating the percentage of glomerular area with positive staining for synaptopodin. *E*: Immunostaining for acetyl-p65 in kidney sections of these mice. *F*: Immunostaining of acetyl-STAT3 in kidney sections of these mice. The quantification data of immunostaining are shown for acetyl-p65 (*G*) and acetyl-STAT3 (*H*). *$P < 0.01$ compared with db/m mice treated with vehicle; #$P < 0.05$ compared with db/db mice treated with vehicle (n = 6). COD, corrected optical density.

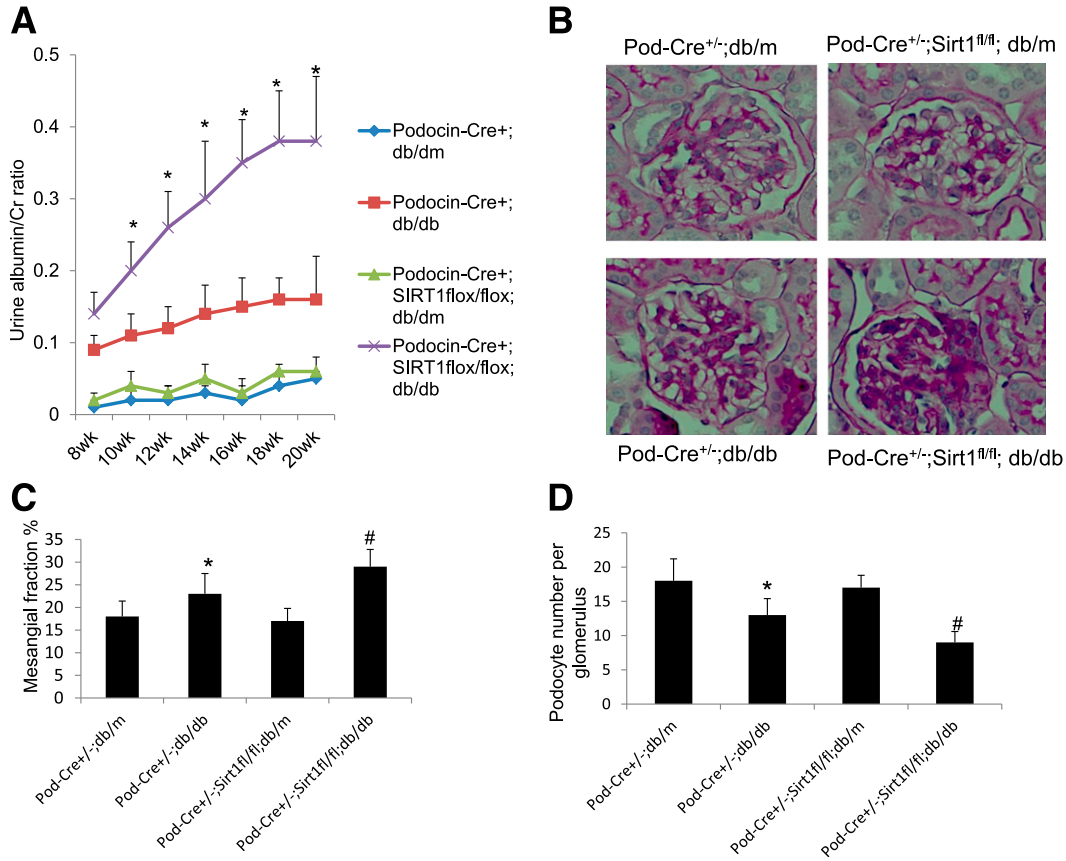

Figure 6—Knockout of *SIRT1* in podocytes aggravates proteinuria and kidney injury in db/db mice. *A*: The urine albumin-to-creatinine ratio was measured as described in QUANTIFICATION OF URINE ALBUMIN. *$P < 0.01$ compared with the corresponding time points of mice in other groups ($n = 6$). *B*: Kidney histology of mice with periodic acid Schiff (PAS) staining. The representative images are shown. *C*: Morphometric analysis was performed in these kidney sections with PAS staining for calculation of mesangial/glomerular fraction area. *D*: Kidney sections also were used for wild-type 1 staining to determine the number of podocytes per glomerulus. *$P < 0.01$ compared with Pod-Cre$^{+/-}$;db/m mice; #$P < 0.05$ compared with Pod-Cre$^{+/-}$;db/db mice ($n = 6$).

in the podocytes of Pod-Cre$^{+/-}$;SIRT1$^{fl/fl}$;db/db mice compared with those of Pod-Cre$^{+/-}$;db/db mice. These data suggest that deletion of SIRT1 specifically in podocytes promotes acetylation of p65 and STAT3, leading to more severe DN.

Effects of Bromodomain Inhibitors on the Development of DN

The above data suggest that acetylation of p65 and STAT3 contributes to the development and progression of DN. Although SIRT1 is known to modulate the acetylation status of these TFs, recent studies suggest that existing SIRT1 agonists may not be specific for SIRT1 (27,28). In addition, SIRT1 agonists may have both protective and harmful effects (29). Therefore, we have developed another approach to modulate TF acetylation as a potential therapy for DN. The bromodomain, which is the conserved structural module present in transcription-associated proteins and histone acetyltransferases, functions as the acetyl-lysine binding domain that is responsible for almost all acetylation-mediated protein-protein interactions in gene transcriptional activation in chromatin (30,31). Our recent study showed that blocking BRD4 association with K310-acetylated p65 using our recently developed small-molecule BET-specific bromodomain inhibitor (MS417) effectively downregulates NF-κB–mediated inflammatory response in kidney cells through inhibition of NF-κB–directed transcriptional activation of cytokines and attenuates kidney injury in HIV-1 transgenic mice (19). The specificity of MS417 on the inhibition of BRD4 binding with acetyl-residue (K310) of p65 also was confirmed in the study (19).

Here, we further confirmed that MS417 also attenuated AGE-induced p65 acetylation and phosphorylation in podocytes (Fig. 7*A* and *B*). Since BRD4 may also interact with acetyl-lysine residues of STAT3, we tested whether MS417 could inhibit STAT3 acetylation. We found that MS417 also inhibited AGE-induced STAT3 acetylation and phosphorylation in podocytes (Fig. 7*C* and *D*). Why the inhibition of acetylation of p65 and STAT3 by MS417 also reduced the phosphorylation of these TFs remains unclear. We speculate that inhibition of p65 and STAT3 acetylation may facilitate dephosphorylation of p65 and STAT3. However, this will need additional confirmation in future studies.

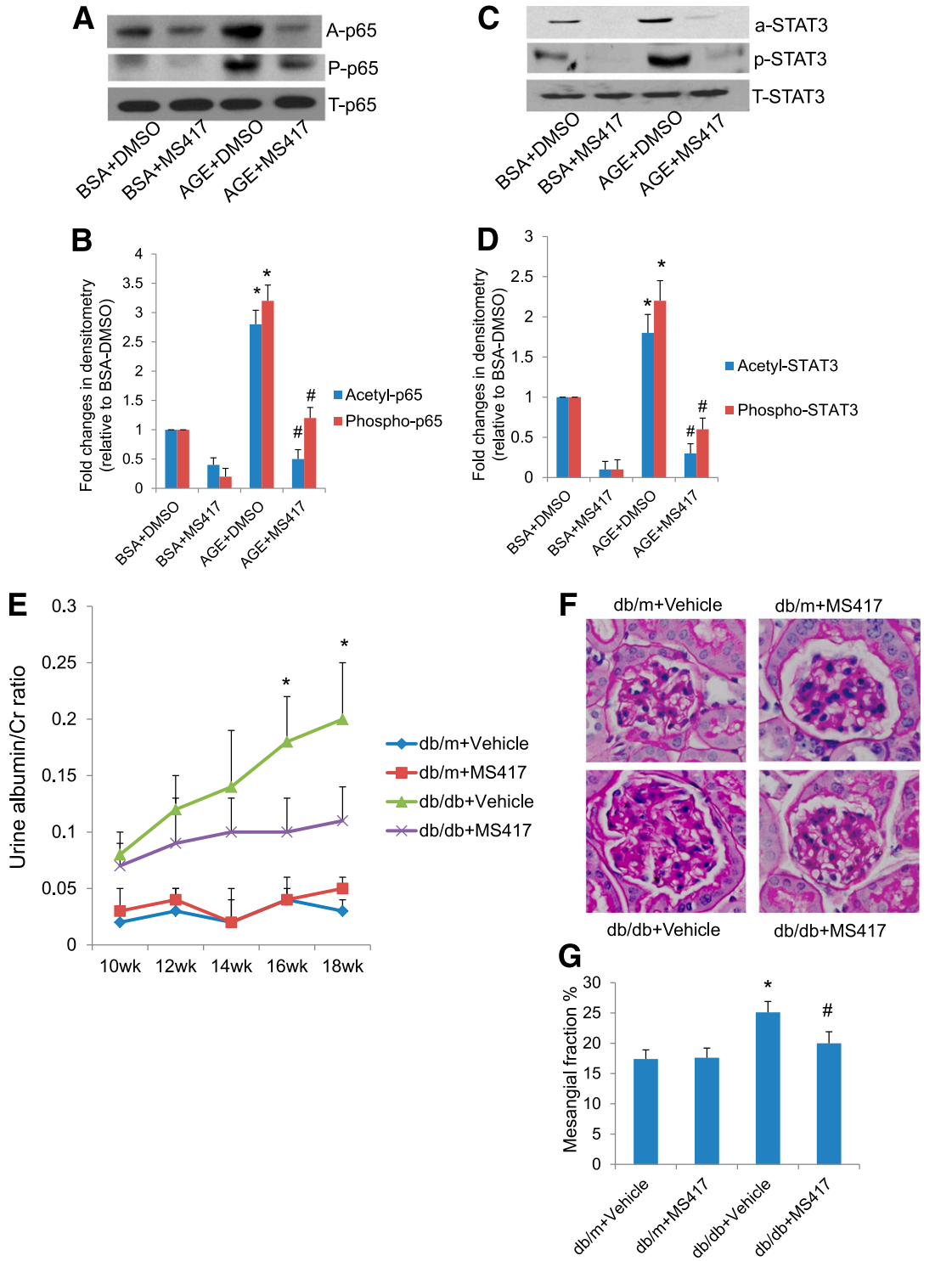

Figure 7—Effects of bromodomain inhibitor in DN. MS417, a bromodomain inhibitor, suppressed acetylation of Stat3 and NF-κB in podocytes treated with AGE. Podocytes were incubated with either BSA or AGE-BSA together with DMSO or MS417 (1.0 μmol/L) for 24 h. Western blot analysis was performed in these cells for acetyl, phosphor- and total p65 (*A*) and STAT3 (*C*). The representative blots of three independent experiments are shown. The densitometry analyses of these Western blots are shown for p65 (*B*) and STAT3 (*D*). The ratios of acetyl-protein or phosphor-protein to total protein were calculated for p65 and STAT3. The fold changes relative to cells treated with BSA + DMSO are shown. *$P < 0.001$ compared with cells treated with BSA + DMSO; #$P < 0.001$ compared with cells treated with AGE-DMSO ($n = 3$). *E*: Db/m and db/db mice were treated with either MS417 or vehicle from 8 weeks to 20 weeks of age (a total of 12 weeks). The urine albumin-to-creatinine ratio was measured as described in QUANTIFICATION OF URINE ALBUMIN. *$P < 0.01$ compared with the corresponding time points of mice from other groups ($n = 6$). *F*: Kidney histology was analyzed after periodic acid Schiff (PAS) staining in these mice. The representative images are shown. *G*: Morphometric analysis was performed in these kidney sections with PAS staining for calculation of mesangial/glomerular fraction area. *$P < 0.05$ compared with vehicle-treated db/m mice; #$P < 0.05$ compared with vehicle-treated db/db mice ($n = 6$).

Next we determined whether MS417 improves kidney injury in diabetic db/db mice. We treated both male db/db and db/m mice with either vehicle or MS417 for a total of 12 weeks. Kidney hypertrophy observed in db/db mice was attenuated by MS417 treatment (Supplementary Table 5). MS417 treatment significantly reduced proteinuria and mesangial expansion in diabetic db/db mice compared with the mice treated with vehicle (Fig. 7*E–G*). The corresponding target genes of NF-κB and STAT3 that increased in the glomeruli of db/db mice also were suppressed by MS417 treatment (Supplementary Fig. 4*A–D*). These data suggest that small-molecule inhibition of the BET bromodomains is a potential novel therapeutic strategy for DN.

DISCUSSION

This is the first study to delineate the role of acetylation of NF-κB and STAT3 as a molecular mechanism of DN. We hypothesized that in diabetic kidneys, TF acetylation is increased because SIRT1 expression is inhibited by AGEs. We confirmed that modulation of TF acetylation—either by inhibition of AGE formation or by directly blocking the interaction between lysine-acetylated TFs and bromodomain-containing proteins—mitigated the development of DN, whereas knockout of SIRT1 in the podocytes aggravated DN (summarized in Fig. 8). Our results strongly support a critical role for downregulation of SIRT1 and hyperacetylation of STAT3 and NF-κB in the pathogenesis of DN. In addition, our studies suggest that several potential interventions could be developed to reduce TF acetylation as potential therapies for DN (Fig. 8).

We found that lysine acetylation is required for transcriptional activation of NF-κB and STAT3. This is consistent with previous studies showing that acetylation of NF-κB is required for transcriptional activation of its target genes (16,32). Previous unbiased analyses reveal that many target genes of NF-κB and STAT3 are activated in DN (7,8). The role of NF-κB and STAT3 in DN also is supported by other studies (33–36). Acetylation of other TFs may also play a role in DN. We have shown a critical role for FOXO4 acetylation in podocyte injury in DN (6). Resveratrol has been shown to reverse acetylation of Smad3 to inhibit transforming growth factor-β1–induced upregulation of collagen IV and fibronectin (37), and Smad3 plays a key role in DN (38). A large body of evidence suggests that p53 mediates the apoptosis of podocytes and tubular epithelial cells in DN (39,40). SIRT1 has been shown to regulate p53 activity by targeting it for deacetylation (41–43). These studies suggest that acetylation of TFs could be a key event leading to DN.

Many studies suggest that SIRT1 affects diseases of aging in mammals, such as diabetes, cancer, and inflammation (44). The role of SIRT1 also has been studied in kidney diseases, including DN (45,46). Hasegawa et al. (47) recently reported that mice with proximal tubular (PT)-specific *SIRT1* knockout developed albuminuria, whereas overexpression of *SIRT1* in PT protected mice from diabetic kidney injury. They demonstrated that the deficiency of *SIRT1* in PT upregulates the expression of claudin-1 in podocytes, which causes podocyte dysfunction, glomerular filtration barrier disruption, and albuminuria in mice. Our mice with podocyte-specific Sirt1 knockout did not develop albuminuria in the basal condition; however, the mice manifested more severe kidney injury when they were diabetic. The discrepancy between these two models suggests that SIRT1 may serve different roles in podocytes and PT. Further studies are required to delineate the cellular mechanism that underlies the phenotypic differences between these two *SIRT1* loss-of-function models.

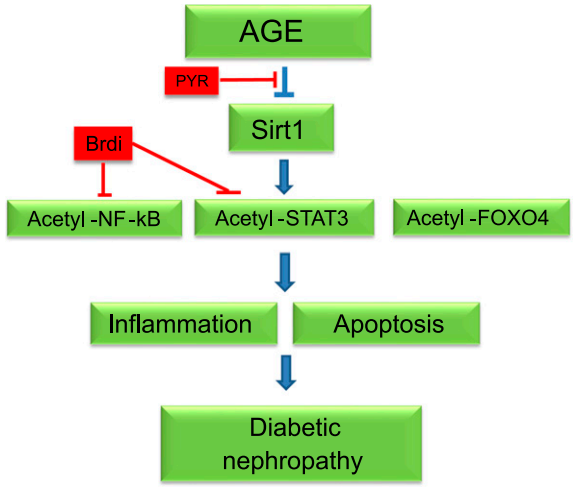

Figure 8—Summary of the role of SIRT1 and acetylation of TFs in DN. AGE suppresses SIRT1 expression, leading to increased acetylation of NF-κB (p65), STAT3, and FOXO4. Acetylated p65 and STAT3 induces the expression of proinflammatory genes in diabetic kidneys. Acetylated FOXO4 induces proapoptotic gene expression, leading to podocyte apoptosis. PYR and bromodomain inhibitors (Brdi) attenuate diabetic kidney injury through the inhibition of AGE formation or by directly inhibiting the acetylation of TFs.

The beneficial effects of SIRT1 likely occur through deacetylation of TFs. Since there are currently no proven specific SIRT1 agonists (27,28), the development of other approaches to modulate TF acetylation is important. Development of small molecules as epigenetic tools to block protein–protein interactions provided by bromodomains is a new therapeutic approach (48). Several cell-permeable small molecules that bind competitively to acetyl-lysine recognition motifs or bromodomains have been developed recently as cancer therapy (49–51). BRD4 belongs to the BET protein family that contains two bromodomains in tandem. Recent studies show that BET proteins play an important role in coordinating gene transcriptional activation in an acetylation-sensitive manner (52). In our previous studies we showed that our BET-specific bromodomain inhibitor (MS417) effectively attenuates NF-κB transcriptional activation of proinflammatory genes in kidney cells and ameliorates inflammation and kidney injury in HIV-1 transgenic mice (Tg26) (19). NF-κB–mediated

inflammation is also a major pathology in DN (7), and our current data suggest that MS417 also inhibited AGE-induced NF-κB acetylation and activation in human podocytes. In addition, MS417 also inhibited STAT3 acetylation, another major pathway involved in DN (8). We confirmed here that MS417 reduces proteinuria and podocyte injury in diabetic db/db mice. In addition, because both NF-κB and STAT3 are key regulators of inflammation and because inflammation is a major contributor to renal fibrosis, we believe that MS417 also will attenuate renal fibrosis in DN. Consistent with this, we demonstrated previously that MS417 treatment improves renal fibrosis in Tg26 mice (19). Taken together, these data suggest that MS417 or its analogs could be developed as a potential new therapy to treat patients with DN.

In summary, our studies suggest that acetylation of NF-κB and STAT3 is increased in diabetic kidneys, contributing to the pathogenesis of DN likely through regulation of the expression of their target genes. Inhibition of AGE restores SIRT1 expression and reduces acetylation of STAT3 and NF-κB, and this is likely one of the mechanisms that AGE inhibitors use to attenuate kidney injury in diabetes. Knockout of *SIRT1* in podocytes aggravates diabetes-induced kidney injury, probably by promoting TF acetylation in podocytes. Finally, we found that BET bromodomain inhibitors, which directly target acetyl-lysine residues of TFs, could be developed as a novel therapeutic approach for treatment of DN. Therefore, our studies provide not only the novel mechanism of but also a potential new therapy for DN.

Funding. J.C.H. is supported by VA Merit Award (1I01BX000345), 973 fund (2012CB517601), and National Institutes of Health (NIH) grants 1R01-DK-078897 and 1R01-DK-088541. P.Y.C. is supported by NIH grant 5K08-DK-082760. Y.Z. is supported by the National Natural Science Foundation of China for Young Investigators (1999-30901944) and the Shanghai Bureau of Health for Young Investigators (2011-XYQ2011059). M.-M.Z. is supported by NIH grants R01-HG-004508 and R01-CA-87658.

Duality of Interest. No potential conflicts of interest relevant to this article were reported.

Author Contributions. R.L., Y.Z., X.L., and H.C. performed the experiments and analyzed the data. B.J. provided human kidney biopsy samples and edited the manuscript. M.-M.Z. provided MS417 and edited the manuscript. P.Y.C. and J.C.H. designed the experiments and wrote the manuscript. J.C.H. is the guarantor of this work and, as such, had full access to all the data in the study and takes responsibility for the integrity of the data and the accuracy of the data analysis.

References

1. Collins AJ, Foley RN, Herzog C, et al. US Renal Data System 2010 annual data report. Am J Kidney Dis 2011;57:A8, e1–526
2. Vlassara H, Striker LJ, Teichberg S, Fuh H, Li YM, Steffes M. Advanced glycation end products induce glomerular sclerosis and albuminuria in normal rats. Proc Natl Acad Sci U S A 1994;91:11704–11708
3. Bohlender JM, Franke S, Stein G, Wolf G. Advanced glycation end products and the kidney. Am J Physiol Renal Physiol 2005;289:F645–F659
4. Zheng F, Cai W, Mitsuhashi T, Vlassara H. Lysozyme enhances renal excretion of advanced glycation endproducts in vivo and suppresses adverse age-mediated cellular effects in vitro: a potential AGE sequestration therapy for diabetic nephropathy? Mol Med 2001;7:737–747
5. Zheng F, Zeng YJ, Plati AR, et al. Combined AGE inhibition and ACEi decreases the progression of established diabetic nephropathy in B6 db/db mice. Kidney Int 2006;70:507–514
6. Chuang PY, Yu Q, Fang W, Uribarri J, He JC. Advanced glycation endproducts induce podocyte apoptosis by activation of the FOXO4 transcription factor. Kidney Int 2007;72:965–976
7. Berthier CC, Zhang H, Schin M, et al. Enhanced expression of Janus kinase-signal transducer and activator of transcription pathway members in human diabetic nephropathy. Diabetes 2009;58:469–477
8. Schmid H, Boucherot A, Yasuda Y, et al.; European Renal cDNA Bank (ERCB) Consortium. Modular activation of nuclear factor-kappaB transcriptional programs in human diabetic nephropathy. Diabetes 2006;55:2993–3003
9. Chuang PY, Dai Y, Liu R, et al. Alteration of forkhead box O (foxo4) acetylation mediates apoptosis of podocytes in diabetes mellitus. PLoS One 2011;6:e23566
10. Brunet A, Sweeney LB, Sturgill JF, et al. Stress-dependent regulation of FOXO transcription factors by the SIRT1 deacetylase. Science 2004;303:2011–2015
11. Motta MC, Divecha N, Lemieux M, et al. Mammalian SIRT1 represses forkhead transcription factors. Cell 2004;116:551–563
12. Bernier M, Paul RK, Martin-Montalvo A, et al. Negative regulation of STAT3 protein-mediated cellular respiration by SIRT1 protein. J Biol Chem 2011;286:19270–19279
13. Nie Y, Erion DM, Yuan Z, et al. STAT3 inhibition of gluconeogenesis is downregulated by SirT1. Nat Cell Biol 2009;11:492–500
14. Sestito R, Madonna S, Scarponi C, et al. STAT3-dependent effects of IL-22 in human keratinocytes are counterregulated by sirtuin 1 through a direct inhibition of STAT3 acetylation. FASEB J 2011;25:916–927
15. Schenk S, McCurdy CE, Philp A, et al. Sirt1 enhances skeletal muscle insulin sensitivity in mice during caloric restriction. J Clin Invest 2011;121:4281–4288
16. Chen Lf, Fischle W, Verdin E, Greene WC. Duration of nuclear NF-kappaB action regulated by reversible acetylation. Science 2001;293:1653–1657
17. Greene WC, Chen LF. Regulation of NF-kappaB action by reversible acetylation. Novartis Found Symp 2004;259:208–217; discussion 218–225
18. Lee JH, Lee B, Lee HS, et al. Lactobacillus suntoryeus inhibits pro-inflammatory cytokine expression and TLR-4-linked NF-kappaB activation in experimental colitis. Int J Colorectal Dis 2009;24:231–237
19. Zhang G, Liu R, Zhong Y, et al. Down-regulation of NF-κB transcriptional activity in HIV-associated kidney disease by BRD4 inhibition. J Biol Chem 2012;287:28840–28851
20. Baelde JJ, Bergijk EC, Hoedemaeker PJ, de Heer E, Bruijn JA. Optimal method for RNA extraction from mouse glomeruli. Nephrol Dial Transplant 1994;9:304–308
21. Mallipattu SK, Liu R, Zheng F, et al. Kruppel-like factor 15 (KLF15) is a key regulator of podocyte differentiation. J Biol Chem 2012;287:19122–19135
22. Saleem MA, O'Hare MJ, Reiser J, et al. A conditionally immortalized human podocyte cell line demonstrating nephrin and podocin expression. J Am Soc Nephrol 2002;13:630–638
23. Makita Z, Vlassara H, Cerami A, Bucala R. Immunochemical detection of advanced glycosylation end products in vivo. J Biol Chem 1992;267:5133–5138
24. Susztak K, Raff AC, Schiffer M, Böttinger EP. Glucose-induced reactive oxygen species cause apoptosis of podocytes and podocyte depletion at the onset of diabetic nephropathy. Diabetes 2006;55:225–233
25. Gassmann M, Grenacher B, Rohde B, Vogel J. Quantifying Western blots: pitfalls of densitometry. Electrophoresis 2009;30:1845–1855
26. Lee TI, Johnstone SE, Young RA. Chromatin immunoprecipitation and microarray-based analysis of protein location. Nat Protoc 2006;1:729–748
27. Beher D, Wu J, Cumine S, et al. Resveratrol is not a direct activator of SIRT1 enzyme activity. Chem Biol Drug Des 2009;74:619–624

28. Pacholec M, Bleasdale JE, Chrunyk B, et al. SRT1720, SRT2183, SRT1460, and resveratrol are not direct activators of SIRT1. J Biol Chem 2010;285:8340–8351
29. Accili D, de Cabo R, Sinclair DA. An unSIRTain role in longevity. Nat Med 2011;17:1350–1351
30. Dhalluin C, Carlson JE, Zeng L, He C, Aggarwal AK, Zhou MM. ^{1}H, 15N and ^{13}C resonance assignments for the bromodomain of the histone acetyltransferase P/CAF. J Biomol NMR 1999;14:291–292
31. Sanchez R, Zhou MM. The role of human bromodomains in chromatin biology and gene transcription. Curr Opin Drug Discov Devel 2009;12:659–665
32. Chen LF, Greene WC. Regulation of distinct biological activities of the NF-kappaB transcription factor complex by acetylation. J Mol Med (Berl) 2003;81:549–557
33. Lu TC, Wang ZH, Feng X, et al. Knockdown of Stat3 activity in vivo prevents diabetic glomerulopathy. Kidney Int 2009;76:63–71
34. Ortiz-Muñoz G, Lopez-Parra V, Lopez-Franco O, et al. Suppressors of cytokine signaling abrogate diabetic nephropathy. J Am Soc Nephrol 2010;21:763–772
35. Lin M, Yiu WH, Wu HJ, et al. Toll-like receptor 4 promotes tubular inflammation in diabetic nephropathy. J Am Soc Nephrol 2012;23:86–102
36. Starkey JM, Haidacher SJ, LeJeune WS, et al. Diabetes-induced activation of canonical and noncanonical nuclear factor-kappaB pathways in renal cortex. Diabetes 2006;55:1252–1259
37. Li J, Qu X, Ricardo SD, Bertram JF, Nikolic-Paterson DJ. Resveratrol inhibits renal fibrosis in the obstructed kidney: potential role in deacetylation of Smad3. Am J Pathol 2010;177:1065–1071
38. Lan HY. Transforming growth factor-β/Smad signalling in diabetic nephropathy. Clin Exp Pharmacol Physiol 2012;39:731–738
39. Niranjan T, Bielesz B, Gruenwald A, et al. The Notch pathway in podocytes plays a role in the development of glomerular disease. Nat Med 2008;14:290–298
40. Brezniceanu ML, Liu F, Wei CC, et al. Catalase overexpression attenuates angiotensinogen expression and apoptosis in diabetic mice. Kidney Int 2007;71:912–923
41. Luo J, Nikolaev AY, Imai S, et al. Negative control of p53 by Sir2alpha promotes cell survival under stress. Cell 2001;107:137–148
42. Milner J, Allison SJ. SIRT1, p53 and mitotic chromosomes. Cell Cycle 2011;10:3049
43. Shah ZH, Ahmed SU, Ford JR, Allison SJ, Knight JR, Milner J. A deacetylase-deficient SIRT1 variant opposes full-length SIRT1 in regulating tumor suppressor p53 and governs expression of cancer-related genes. Mol Cell Biol 2012;32:704–716
44. Donmez G, Guarente L. Aging and disease: connections to sirtuins. Aging Cell 2010;9:285–290
45. Hao CM, Haase VH. Sirtuins and their relevance to the kidney. J Am Soc Nephrol 2010;21:1620–1627
46. Kume S, Thomas MC, Koya D. Nutrient sensing, autophagy, and diabetic nephropathy. Diabetes 2012;61:23–29
47. Hasegawa K, Wakino S, Simic P, et al. Renal tubular Sirt1 attenuates diabetic albuminuria by epigenetically suppressing Claudin-1 overexpression in podocytes. Nat Med 2013;19:1496–1504
48. Mujtaba S, Zeng L, Zhou MM. Structure and acetyl-lysine recognition of the bromodomain. Oncogene 2007;26:5521–5527
49. Filippakopoulos P, Qi J, Picaud S, et al. Selective inhibition of BET bromodomains. Nature 2010;468:1067–1073
50. Zuber J, Shi J, Wang E, et al. RNAi screen identifies Brd4 as a therapeutic target in acute myeloid leukaemia. Nature 2011;478:524–528
51. Delmore JE, Issa GC, Lemieux ME, et al. BET bromodomain inhibition as a therapeutic strategy to target c-Myc. Cell 2011;146:904–917
52. Chiang CM. Brd4 engagement from chromatin targeting to transcriptional regulation: selective contact with acetylated histone H3 and H4. F1000 Biol Rep 2009;1:98